Available online at www.sciencedirect.com
SCIENCE DIRECT®
Engineering Structures 27 (2005) 1040–1051
ENGINEERING STRUCTURES
www.elsevier.com/locate/engstruct

An analytical model for stress–strain behavior of confined concrete

Baris Binici*

Middle East Technical University, Department of Civil Engineering, İnönü Bulvarı, 06531 Ankara, Turkey

Received 28 September 2004; received in revised form 17 February 2005; accepted 17 February 2005
Available online 15 April 2005

Abstract

It is well known that the strength and ductility of concrete are highly dependent on the level of confinement provided by the lateral reinforcement. The stiffness and the constitutive behavior of the confining reinforcement (elastic, elastoplastic, etc.) are the important factors affecting the behavior of concrete. In this study, a new simple confined concrete model is developed for describing the axial and lateral deformation characteristics of concrete under triaxial compression. The stress–strain relationship of confined concrete in the axial direction is defined with an elastic region followed by a nonlinear curve. The descending region of the stress–strain curve is defined using a constant failure energy criterion. The elastic limit, ultimate strength, and residual capacity of confined concrete are determined using the Leon–Pramono criterion. The lateral deformation of confined concrete is described using a function that provides a smooth transition from elastic to inelastic behavior and satisfies the zero volumetric strain condition at ultimate strength. The model estimations are compared with the results of triaxial concrete compression tests, and fiber reinforced polymer (FRP) and steel confined concrete tests reported in the literature. A good agreement was observed in terms of ultimate strength, residual strength, and axial and lateral deformation behavior. It was observed that the model can be successfully applied for FRP and steel confined concrete, removing the need to adjust parameters for different lateral reinforcement types. Finally, a parametric study was conducted to investigate the effect of the lateral reinforcement ratio, concrete strength, and compressive failure energy on the behavior of steel and FRP confined concrete.

Keywords: Concrete; Confinement; Fiber reinforced polymers

1. Introduction

Reinforced concrete columns and bridge piers are provided with lateral reinforcement to increase the strength and ductility of these members especially when subjected to earthquake induced forces. On the other hand, the use of fiber reinforced polymers to increase the axial load carrying capacity of deficient columns has gained increasing popularity within the last decade. Furthermore, concrete filled steel tubes where the axial load is solely carried by concrete confined by steel tubes [1,2] offer excellent structural systems where both materials are utilized efficiently. The design and detailed analyses of these members can be performed in safe and economic ways as long as a thorough understanding of the confining reinforcement–concrete interactions is available along with models that are capable of representing confined concrete behavior.

Since the recognition of strength gain in concrete as a result of confining reinforcement [3], there has been a tremendous effort to understand and model confined concrete behavior. Some of the earlier models were based on biaxial compression experiments [4–7] whereas some were based on limited experimental evidence regarding softening behavior of confined concrete [8]. Recent triaxial compression experiments [9–13] provided an extended database on compressive behavior of concrete that can be used to develop and verify confined concrete models.

Models for describing axial stress–strain behavior of steel confined concrete have been developed on the basis of an extensive database of experimental research [14–16]. In these models the ultimate strength and the descending region of the stress–strain curves have been adjusted as a function of confinement provided by the lateral

* Tel.: +90 312 210 2457; fax: +90 312 210 1193.
E-mail address: binici@metu.edu.tr.

0141-0296/$ - see front matter © 2005 Elsevier Ltd. All rights reserved.
doi:10.1016/j.engstruct.2005.03.002

reinforcement ratio and uniaxial compressive strength. The simplicity of these models has made them popular for use in capacity calculations and sectional analyses. One important disadvantage of these models is their lack of generality. They are applicable to only steel confined concrete where the confining reinforcement can be approximated by an elastic–perfectly plastic relationship and peak strength is achieved when the lateral reinforcement yields. With recent advances in high strength concrete and high strength steel and with the use of composite materials (i.e. fiber reinforced polymers (FRPs)) as confining reinforcement, these models require further calibrations to overcome their limitations. This motivated the development of other models for normal and high strength concrete [17,18] and FRP confined concrete [19,20]. Another important drawback of these models is the lack of objectivity in the softening regime. No matter what kind of function is selected for the softening region, as long as localization is not taken into account, the softening region will exhibit a size effect and objective results cannot be achieved [21]. The verification of this argument has been observed in many uniaxial compression experiments [22,23]. The simplest way of regularizing the compressive softening region approximately, which is usually used in finite element analyses, is based on a constant fracture energy criterion similar to that applied for tensile cracking of concrete [24]. Furthermore, the importance of estimating lateral strains to define 'failure' is appreciated when failure is dictated by the rupture of the confining reinforcement or loss of lateral restraint causing buckling of longitudinal bars.

Plasticity based models provide a convenient description of the hardening, softening, and dilatation behavior of concrete and they are generally used together with a constitutive driver or within finite element analysis [25–27]. For the analyses of structures with complicated geometry and boundary conditions, finite element analysis methods using concrete plasticity models are excellent tools [27]. However, in order to estimate accurately the load–deformation behavior of axially loaded concrete members confined with materials having different constitutive relationships, simpler models may be preferred by structural engineers in the preliminary design of these members. At the heart of the problem remains the realistic description of the behavior of concrete subjected to triaxial compression. Once this is established any passive or active confining mechanism can be simulated. The objective of this research is to provide one such model and to verify it for steel and FRP confined concrete subjected to axial compression. It is believed that the proposed model can be useful in the preliminary design of steel confined columns or in the fiber reinforced polymer retrofit design of deficient columns.

2. Model description

First, the phenomenological model is described in this section. The model is a global representation rather than a local one for axially loaded concrete subjected to constant confinement. Then, the procedure for obtaining the behavior of columns with passive confinement (columns provided with steel or fiber reinforced polymers) by satisfying lateral strain compatibility between concrete and the reinforcing jacket for the axial loading history is presented. Since the model can be thought of as a single element representation of concrete subjected to compression, the strains used below are average quantities over the specimen rather than actual strains. After localization starts, strain distribution along the specimen height is no longer uniform [28]. Instead of tracing this non-uniform strain distribution, average strain values are used in the description below such that average stress–strain behavior of a confined column can be obtained.

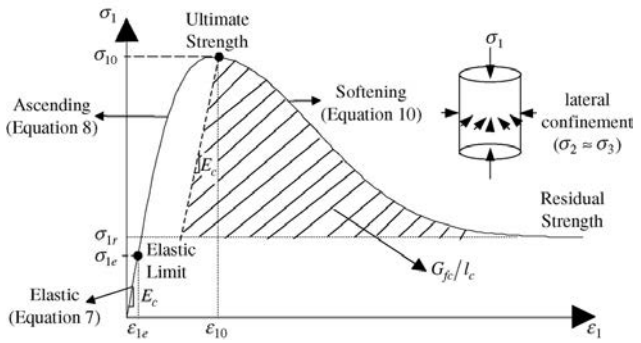

Fig. 1. Confined concrete stress–strain curve.

2.1. Axial deformations

For the present discussion, axial and lateral directions are denoted by 1 and 3, respectively. It is assumed that stresses and strains are similar in the two lateral directions ($\sigma_2 \approx \sigma_3, \varepsilon_2 \approx \varepsilon_3$). Furthermore, compressive stresses and strains are assumed to be positive whereas volume expansion is taken as negative. The axial stress–strain response of concrete confined by constant lateral pressure can be described using three distinct locations on the stress–strain curve (Fig. 1):

(1) The elastic limit up to which concrete is assumed to be isotropic and linear elastic ($\sigma_{1e}, \varepsilon_{1e}$).

(2) The ultimate strength which is a function of lateral pressure, ($\sigma_{10}, \varepsilon_{10}$).

(3) The residual capacity remaining as a result of internal friction, (σ_{1r}).

In order to define these points on the stress–strain curve, a loading surface named hereafter the Leon–Pramono criterion (LPC) [25] is used as given in Eq. (1):

$$\left[(1-k)\left(\frac{\sigma_3}{f'_c}\right)^2 + \frac{\sigma_1-\sigma_3}{f'_c}\right]^2 + k^2 m\left(\frac{\sigma_3}{f'_c}\right) - k^2 c = 0. \tag{1}$$

Above, k is the hardening parameter and is equal to 0.1 at the elastic limit, and it is equal to one at ultimate strength and in

the softening region. σ_1 is the axial stress, σ_3 is the confining stress, and f'_c is the uniaxial compressive strength. c is the softening parameter and is equal to one in the hardening region and zero for residual strength. The constant parameter

$$m = \frac{f_c'^2 - f_t'^2}{f'_c f'_t} \tag{2}$$

depends only on the uniaxial compressive strength f'_c and uniaxial tensile strength f'_t. The LPC given in Eq. (1) combines the one parameter Mohr–Coulomb friction law and the Rankine criterion with a tension cut-off condition. It omits the effect of intermediate principal stress; therefore it is attractive for use for cases where confining stresses in lateral directions are similar (i.e. axially loaded columns). Furthermore, since the elastic limit and ultimate and residual strength are expressed directly in terms of stress components, the need to calculate stress invariants is eliminated. Assuming compression positive, Eq. (1) can be rearranged to express σ_1 as a function of the confinement ratio and model parameters in the following form:

$$\sigma_1 = f'_c \left(k\sqrt{c + m\phi} - (1-k)\phi^2 + \phi \right) \tag{3}$$

where ϕ is the confinement ratio (σ_3/f'_c). Ultimate and residual strength envelopes obtained using Eq. (3) and the above mentioned values for k and c are compared to experimentally observed strength values in Fig. 2. It should be noted that a uniaxial tensile strength value of $0.1\,f'_c$ yielding an m value of 9.9 is used in Eq. (3). It can be observed that the LPC provides a reasonably good estimate of the ultimate strength and residual capacity. Experiments that extend well into the softening regime where the capacity stabilizes at the residual strength are included in Fig. 2(b). Eq. (3) has a cap for the elastic limit ($k = 0.1, c = 1$), meaning that beyond a certain level of confinement ratio ($\phi \geq 0.65$), the elastic limit stress (σ_{1e}) starts to decrease. The stress–strain curve described here assumes that failure does not occur as a result of lateral confining stress prior to the application of the axial stress. This assumption is never violated as long as the lateral pressure is smaller than the biaxial compressive strength prior to application of the axial compressive stress or there is a passive confinement mechanism, which is activated by the application of the axial stress.

Imran and Pantazopoulou [10] reported that the confinement ratio for the brittle to ductile transition depends on the water–cement ratio and varies between 0.2 and 0.6. Pivonka et al. [27] suggested using a value of 0.28 according with data provided by Hurlbut. Smith et al. [9] reported that the residual strength is equal to the ultimate strength for a confinement level of about 0.6. In this study, a confinement ratio of 0.4 is taken as the transition point beyond which no softening occurs, and a perfectly plastic behavior is achieved. This average value is believed to represent the transition point with sufficient accuracy.

Once the elastic limit stress is known, the elastic limit strain (ε_{1e}) can be calculated using Hooke's law given by

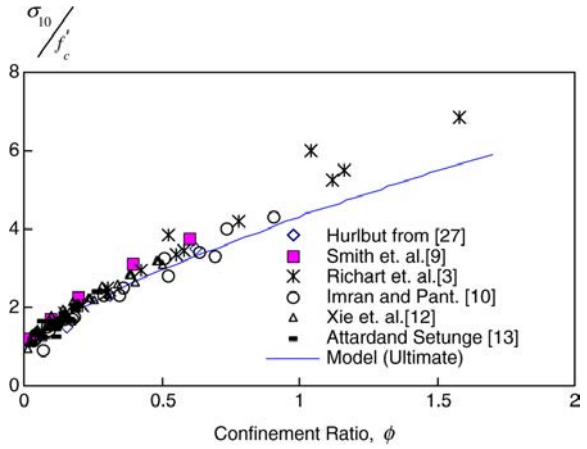

(a) Ultimate strength.

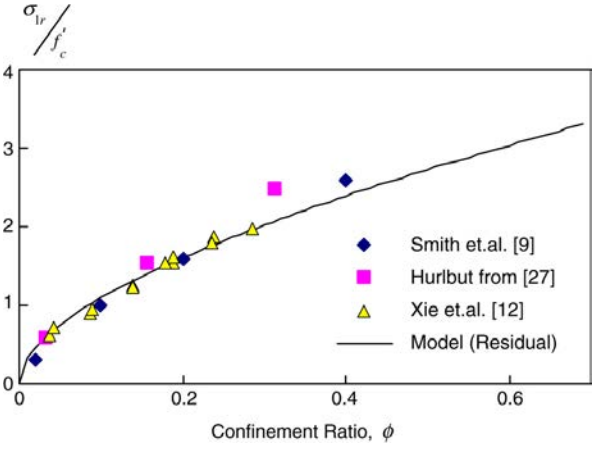

(b) Residual strength.

Fig. 2. Comparisons of experiments and model predictions for ultimate and residual strength values.

Eq. (4) where E_c is the modulus of elasticity of concrete that is calculated according to ACI 318M-02 [29] ($E_c = 4750\sqrt{f'_c}$ in MPa):

$$\varepsilon_{1e} = \frac{\sigma_{1e}}{E_c}. \tag{4}$$

The strain at ultimate stress in a triaxial compression test (ε_{10}) is calculated using the following relationship proposed by Richart et al. [3]:

$$\varepsilon_{10} = 5\varepsilon_o \left(\frac{\sigma_{10}}{f'_c} - 0.8 \right). \tag{5}$$

In Eq. (5), the strain at peak stress under uniaxial compression (ε_o) is calculated according to the relationship in Eq. (6) proposed by Tasdemir et al. [30] on the basis of regression analyses of 228 uniaxial compression test specimens with uniaxial compressive strength values ranging from 6 to 105 MPa:

$$\varepsilon_o = (-0.067\,f_c'^2 + 29.9\,f'_c + 1053)10^{-6}. \tag{6}$$

The curve defining the complete stress–strain relationship is defined with three separate relations in the elastic,

hardening, and softening regions. In the elastic region, the axial stress–strain relationship is given by Hooke's law:

$$\sigma_1 = E_c \varepsilon_1 \qquad \text{for } \varepsilon_1 \le \varepsilon_{1e}. \tag{7}$$

Beyond the elastic limit, the ascending part of the stress–strain curve is described by

$$\sigma_1 = \sigma_{1e} + (\sigma_{10} - \sigma_{1e}) \left(\frac{\varepsilon_1 - \varepsilon_{1e}}{\varepsilon_{10} - \varepsilon_{1e}} \right) \frac{r}{r - 1 + \left(\frac{\varepsilon_1 - \varepsilon_{1e}}{\varepsilon_{10} - \varepsilon_{1e}} \right)^r}$$
$$\text{for } \varepsilon_{1e} \le \varepsilon_1 \le \varepsilon_{10} \tag{8}$$

which is a modified form of the Popovics curve [31]. The constants r and E_s are given as

$$r = \frac{E_c}{E_c - E_s} \qquad \text{and} \qquad E_s = \frac{\sigma_{10} - \sigma_{1e}}{\varepsilon_{10} - \varepsilon_{1e}}. \tag{9}$$

The descending region is described by

$$\sigma_1 = \sigma_{1r} + (\sigma_{10} - \sigma_{1r}) \exp \left[- \left(\frac{\varepsilon_1 - \varepsilon_{10}}{\alpha} \right)^2 \right]$$
$$\text{for } \varepsilon_{10} \le \varepsilon_1 \tag{10}$$

which is an exponential softening function. A similar function has previously been used by Pivonka et al. [27] in a multi-surface plasticity model to describe concrete softening. Parameter α in Eq. (9) is calibrated such that the area under the softening region (including the elastic unloading portion as shown in Fig. 1) is equal to the compressive failure energy obtained from a uniaxial compression test divided by the characteristic length of the specimen in the loading direction (G_{fc}/l_c). This assumption implies that the model described herein should be thought of not as a true material law but as a phenomenological model that incorporates the size of the specimen under consideration. Hence, the strains used in the above derivation are average values rather than actual ones, which would show non-uniformity after localization depending on their locations (localization and unloading zones). The equality given in Eq. (11) yields the value of α given by Eq. (12):

$$G_{fc} = l_c \left\{ \int_{\varepsilon_{10}}^{\infty} (\sigma_{10} - \sigma_{1r}) \exp \left[- \left(\frac{\varepsilon_1 - \varepsilon_{10}}{\alpha} \right)^2 \right] \mathrm{d}\varepsilon_1 + \frac{(\sigma_{10} - \sigma_{1r})^2}{2E_c} \right\} \tag{11}$$

$$\alpha = \frac{1}{\sqrt{\pi}(\sigma_{10} - \sigma_{1r})} \left(\frac{2G_{fc}}{l_c} - \frac{(\sigma_{10} - \sigma_{1r})^2}{E_c} \right). \tag{12}$$

In this fashion, it is possible to approximately regularize the softening region by ensuring that the same amount of energy is dissipated during softening behavior for different length specimens. Here, it is assumed that localization initiates when peak stress is reached under axial loading. Uniaxial compression experiments performed by Shah and Sankar [28] show that the extent of cracking up to about 85% of the peak stress is due to bond cracks in the loading and transverse directions. Beyond this point, these cracks coalesce into continuous cracks resulting in a significant volume expansion of the specimen. Torrenti et al. [32] made a similar observation using stereophotogrammetry and stated that localization occurs at maximal stress for plain concrete under uniaxial compression. As the experimental evidence suggests, it is not unrealistic to assume localization starting nearly at the peak stress for uniaxial compression. A similar assumption regarding the initiation of strain localization was utilized by Cusson et al. [33] for steel confined concrete under axial compression in their confined concrete model. However, it may be argued that the triaxial state of stress may inhibit the onset of localization compared to uniaxial compression. Experiments conducted by Sfer et al. [34] show that there is distributed microcracking and several macrocracks leading to a softening response in uniaxial compression. Conversely, in constant confined concrete tests, no distributed cracking was observed and failure was due to the propagation of a few macrocracks. The residual capacity was attributed to the friction between these macrocracks. Analytical examinations of failure modes (diffusive versus localized) have been presented by Kang and Willam [35] and Yoshikawa and Yamakawa [36] using plasticity models. These results show that failure is diffusive for low confinement whereas it is localized for high confinement regions. These results agree well with the observed damage of concrete specimens [34]. Since either failure type (diffusive versus localized) implies a discontinuity at the material level, no distinction is made between them in this study. Furthermore, development of appropriate regularization techniques for these two cases is beyond the scope of this study. Hence, the same energy regularization is applied for low and high confinement cases. This assumption, although it may not necessarily reflect reality, is very easy to implement for use in practical engineering models. The experimental confirmation of the model presented in the following sections also supports the adopting of such an approach.

It should also be noted that Eqs. (7), (8) and (10) that define the complete stress–strain curve for confined concrete loaded in the 1 direction satisfy C^1 continuity (values and slopes are continuous) requirements, which is successful in reproducing the experimental results.

2.2. Transverse deformations

Deformations in the transverse direction are described using the secant strain ratio, υ_s ($\upsilon_s = -\varepsilon_3/\varepsilon_1$). In the elastic region the secant strain ratio is equal to Poisson's ratio of concrete (υ_0) which is usually between 0.15 and 0.2. In the elastic range, the secant strain ratio is given by

$$\upsilon_s = \upsilon_0 \qquad \text{for } \varepsilon_1 \le \varepsilon_{1e}. \tag{13}$$

At ultimate strength, Imran and Pantazopoulou [10] observed that the volume expansion is approximately zero in their triaxial compression experiments, meaning that the secant strain ratio attains a value of 0.5 since the lateral

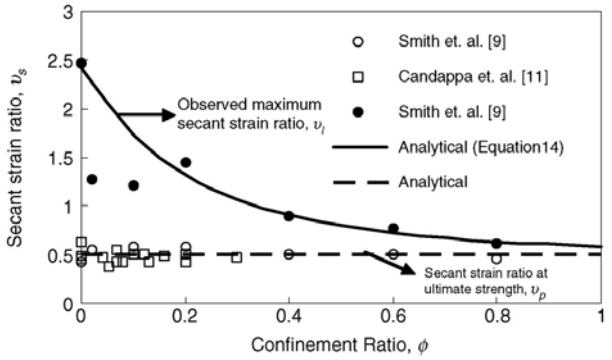

Fig. 3. Secant strain ratios at ultimate strength and maximum deformations.

strains in the 2 and 3 directions are similar. Secant strain ratios at ultimate strength from triaxial compression tests made by various researchers are plotted as a function of confinement ratio in Fig. 3. It can be observed that secant strain ratios are populated around 0.5 and are independent from the confinement ratios. Therefore, it is reasonable to state that the secant strain ratio at peak strength (υ_p) should be 0.5, corresponding to no volume expansion.

Beyond the ultimate strength, the evolution of the secant strain ratio depends on the level of confinement. From experiments of Smith et al. [9] that extend well into the softening region (up to 10 times the strain at uniaxial compressive strength), a plot where largest secant strain ratios are given as a function of the confinement ratio appears in Fig. 3. It can be observed that the largest secant strain ratio decreases with increasing confinement ratio. The largest secant strain ratios can be obtained from

$$\upsilon_l = \upsilon_p + \frac{1}{(\phi + 0.85)^4} \tag{14}$$

as a function with the best fit to the experimentally observed values. In summary, the secant strain ratio is constant and equal to Poisson's ratio in the elastic range. At ultimate strength, it is equal to υ_p, whereas it approaches a limiting value (υ_l) for strains well beyond the strain at peak stress. A function that satisfies these and the continuity requirements is

$$\upsilon_s = \upsilon_l - (\upsilon_l - \upsilon_0) \exp\left[-\left(\frac{\varepsilon_1 - \varepsilon_{1e}}{\Delta}\right)^2\right] \quad \text{for } \varepsilon_{1e} \le \varepsilon_1 \tag{15}$$

where the parameter

$$\Delta = \frac{\varepsilon_{10} - \varepsilon_{1e}}{\sqrt{-\ln \beta}} \qquad \text{and} \qquad \beta = \frac{\upsilon_l - \upsilon_p}{\upsilon_l - \upsilon_0} \tag{16}$$

is calibrated such that when ε_1 is equal to ε_{10}, the secant strain ratio is equal to υ_p. Eq. (15) implies that the length of the localized zone in the transverse direction is similar to the specimen width; therefore the secant strain ratio is independent of the lateral size of the specimen. This assumption has previously been made by Borges et al. [37] in the analysis of concrete specimens subjected to uniaxial compression and flexure. In reality, lateral strains in the localized zone are certainly different to the lateral strains outside of this zone. However, to the knowledge of the author, there are no experimental results reported for the length of the localized zone in the lateral direction at various stress levels for triaxial compression tests. Therefore, a simpler approach is preferred in this study where the secant strain ratios are directly extracted from the results of triaxial compression tests. For a more detailed analysis accounting for this effect, a discretized solution (such as the finite element method) is necessary. This is beyond the scope of the model developed herein, which is intended to be a practical one for estimating load carrying and deformation capacities of axially loaded concrete columns.

The secant strain relationships given by Eqs. (14) and (15) define the lateral deformations as a function of confinement ratio and axial strain. Imposing an upper bound equal to the experimentally derived value of the limiting secant strain ratio, excessive dilatation is avoided. Once the secant strain ratio is known, the lateral strain can be computed from Eq. (17):

$$\varepsilon_3 = -\upsilon_s \varepsilon_1. \tag{17}$$

2.3. Calculations for constant and passive confined concrete

The input parameters for obtaining complete stress–strain behavior in the axial and lateral directions are the uniaxial compressive strength, f'_c, uniaxial tensile strength, f'_t, compressive failure energy, G_{fc}, length of the specimen in the loading direction, l_c, and Poisson's ratio, υ_0. For all practical purposes the uniaxial tensile strength, f'_t, can be taken as 10% of the uniaxial compressive strength, f'_c, and υ_0 can be assumed as 0.20, reducing the number of parameters required to three.

Concrete subjected to constant confinement throughout the axial loading is mostly encountered in triaxial compression experiments. In order to obtain the complete stress–strain curves for this case, axial strains are imposed. Since the level of confinement is constant throughout the axial loading, elastic limit, ultimate strength, the corresponding strains and the residual strength are obtained using Eqs. (3)–(5). Then the stress–strain curves in the axial directions are obtained according to Eqs. (7), (8) and (10). Lateral strains corresponding to the prescribed axial strains are computed using Eq. (17) in which the secant strain ratios, υ_s, are calculated using Eqs. (13) and (15).

For cases where confinement is provided with the use of a confining jacket, strain compatibility in the lateral direction is enforced for the imposed axial strain such that jacket and lateral concrete strains are similar. On this basis, the following procedure is applied:

(a) Impose the axial strain, ε_1.

(b) Compute the lateral pressure, σ_3, such that the lateral strain in the jacket is equal to the lateral strain of concrete.

This requires the following nonlinear equation to be solved for σ_3:

$$\varepsilon_1 \upsilon_s(\sigma_3) - \sigma_3/D = 0. \quad (18)$$

In Eq. (18), $\upsilon_s(\sigma_3)$ is the secant strain ratio given by Eq. (15) in the inelastic range, and it is a function of σ_3 since υ_l is in turn a function of the confinement ratio ($\phi = \sigma_3/f'_c$). D is the effective jacket rigidity given by

$$D = \frac{E_j t}{R} = \frac{E_j \rho_j}{2} \quad (19)$$

where E_j is the modulus of elasticity of the jacket in the hoop direction, t is the thickness of the jacket, R is the radius of the confined concrete section, and ρ_j is the volumetric ratio of the jacket (the ratio of the lateral reinforcement volume to the ratio of concrete volumes). If the lateral reinforcement has a yield strength f_y and an elastic perfectly plastic behavior, σ_3 cannot be greater than σ_{max} ($\sigma_3 \leq \sigma_{max} = f_y t/R$).

(c) Compute the axial stress corresponding to the imposed axial strain when subjected to a confining stress, σ_3.

(d) Repeat (a)–(c) for all ε_1 or until a prescribed ultimate value of ε_3 is reached.

The analysis procedure described above considers the confining jacket–concrete interaction for jackets exhibiting linear elastic and elastic perfectly plastic behavior. The iterative part of the procedure, which can be handled using single point iterations, is solving Eq. (18) in order to compute the level of confinement that satisfies compatibility. In this way, the behavior of passive confined concrete is obtained from a family of curves describing concrete behavior under constant confinement.

3. Model verification

3.1. Constant confinement

Triaxial compression tests [9–12] were used for verification of the model. The input parameters used in the analyses and the comparisons of analysis results with experimental curves are presented in Figs. 4–7. The uniaxial compressive strength and specimen length are well documented in these studies. However, the compressive failure energy was not reported or the test was terminated prior to obtaining the complete softening regime. When the complete uniaxial compression stress–strain curves were known, the compressive failure energy was computed by multiplying the area under the softening region by the specimen length (Eq. (11)). Otherwise, the compressive failure energy that matches the slope of the descending region was obtained by trial and error. Comparisons are made for both axial and lateral strains whenever both were reported.

Comparisons of analytical results with experiments [10] are given in Fig. 4. Plots shown in this figure refer to the average axial strains after the application of confining

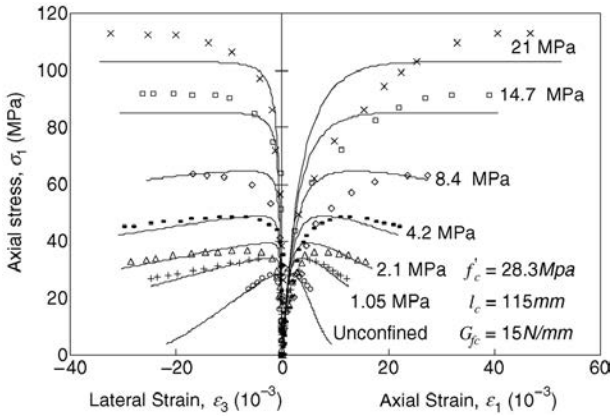

Fig. 4. Comparisons of experimental results of Imran and Pantazopoulou [10] with analysis results (points are the experimental results, lines are analytical estimations, numbers next to curves are confining stresses).

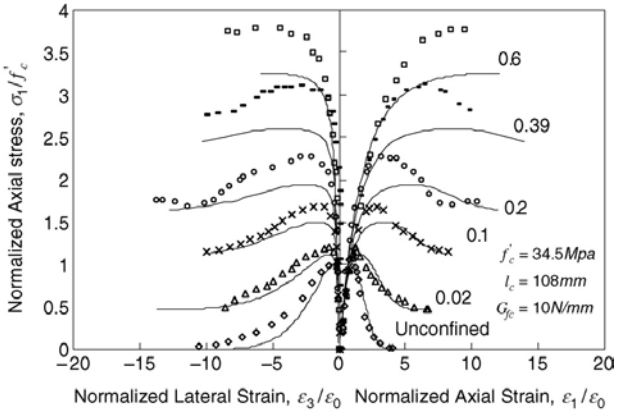

Fig. 5. Comparisons of experimental results of Smith et al. [9] with analysis results (points are the experimental results, lines are analytical estimations, numbers next to curves are confinement ratios).

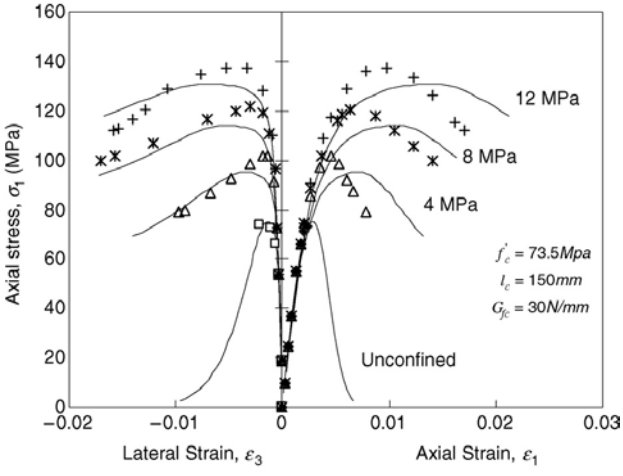

Fig. 6. Comparisons of experimental results of Candappa et al. [11] with analysis results (points are the experimental results, lines are analytical estimations, numbers next to curves are confining stresses).

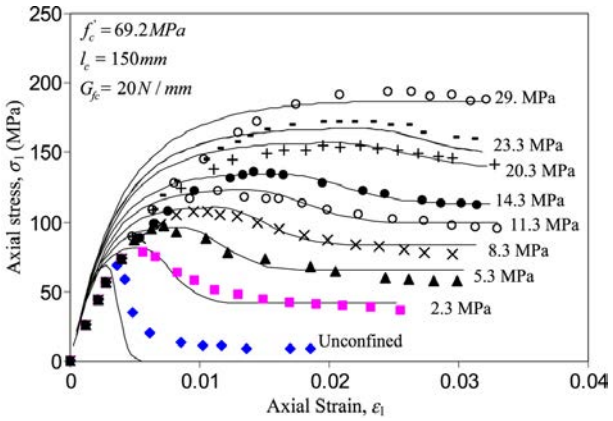

Fig. 7. Comparisons of experimental results of Xie et al. [12] with analysis results (points are the experimental results, lines are analytical estimations, numbers next to curves are confining stresses).

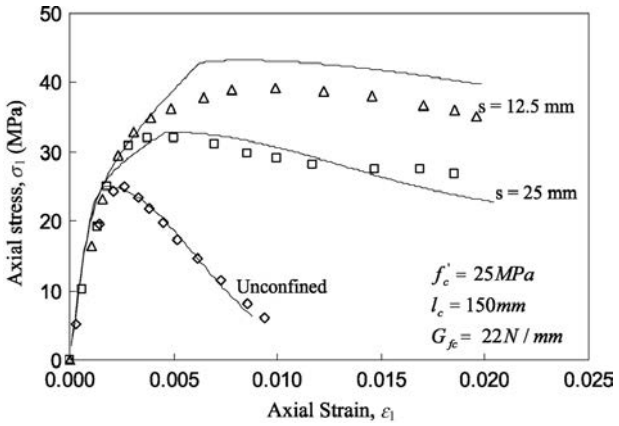

Fig. 8. Comparisons of experimental results of Ahmad and Shah [8] with analysis results for concrete confined with steel spirals ($f_c' = 25$ MPa; points are the experimental results, lines are analytical estimations).

stresses. In other words, the state after the application of the confining stress is taken as the reference state of zero strain and plotted strains are actually the measured strain increments with respect to this state. A good agreement was observed for the axial and lateral behavior especially at low levels of confinement. Ultimate strength estimations were found to be satisfactory for all confinement levels. At high levels of confinement, the ascending regions of axial stress–strain curves were slightly overestimated. Comparisons of analytical curves with experiments reported by Smith et al. [9] are given in Fig. 5. Ultimate strength estimations at low levels of confinement were excellent, whereas strength underpredictions can be observed at higher levels of confinement. In general, the model is capable of tracing the axial and lateral behavior with sufficient engineering accuracy. Triaxial compression tests for higher strength concrete performed by Candappa et al. [11] and Xie et al. [12] were compared with analytical curves in Figs. 6 and 7. An adequate estimation of the triaxial behavior of concrete was observed for both results. The initial stiffness of the experiments by Xie et al. [12] was overestimated, whereas an excellent agreement was observed between the ultimate and residual capacity estimations and experimental results. From all of these comparisons it is possible to say that the model has the capability to estimate strength, deformation capacity, residual strength, and transverse behavior with acceptable accuracy, retaining a very simplistic approach.

3.2. Steel confined concrete

The analysis results for concrete confined with the use of steel spirals and steel tubes were compared with the experimental results of Ahmad and Shah [8] and Lahlou et al. [38]. Ahmad and Shah [8] tested concrete cylinders (75 mm × 150 mm) in axial compression reinforced laterally with steel spirals. Spirals with the yield strength of 414 MPa were placed flush to the molds, resulting in practically no cover. Spacing of the spirals and concrete uniaxial compressive strength were the main test variables. The following equation [8] was used to account for the equivalency between discrete lateral reinforcement and a continuous jacket:

$$t = \frac{A_s}{s}\left(1 - \sqrt{\frac{s}{1.25D_s}}\right). \tag{20}$$

In Eq. (20), t is the thickness of the equivalent continuous jacket to be used in Eq. (19), A_s is the cross-sectional area of the spiral, s is the spacing of the spiral, and D_s is the diameter of the specimen. This relationship was deduced from the observation that when the spiral spacing is greater than 1.25 times that of D_s, the effect of confinement is negligible.

The axial stress–strain response of the specimens is compared to the analytical estimates in Figs. 8 and 9. A satisfactory agreement as regards ultimate strength and slope of the descending branch is observed. Furthermore, the effect of spiral spacing on the strength and ductility is accounted for using the proposed model.

Another way of utilizing steel as confining reinforcement is by using steel tubes that do not directly carry axial load, but serve as confining reinforcement. This type of concrete filled steel tube system (CFST) was found to be very efficient in terms of utilizing concrete compressive strength together with ductile behavior of steel tube [1, 2]. Despite lubrication of the inner side of the tube to avoid friction, the steel tube was observed to be stressed in tension in the hoop direction and in compression in the axial direction [2]. The relationship between axial and lateral strains in the tube was found to be proportionally increasing, and the stresses at tube yielding in both directions were approximately similar. Experiments on circular CFST (150 mm × 300 mm) where only concrete was loaded in the axial direction were presented by Lahlou [38]. The yield strength of tube was modified to account for the equal biaxial tension–compression loading of the tube

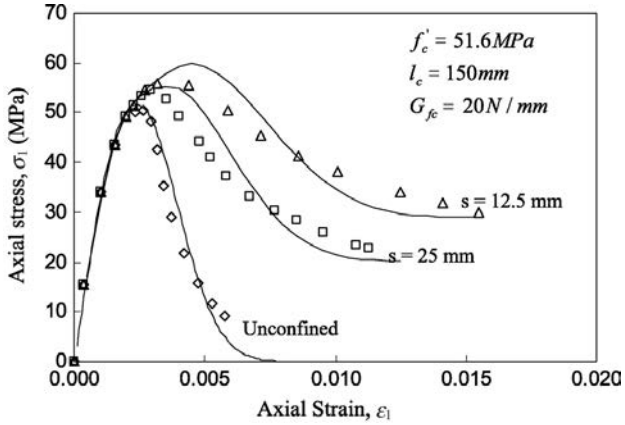

Fig. 9. Comparisons of experimental results of Ahmad and Shah [8] with analysis results for concrete confined with steel spirals ($f_c' = 51.6$ MPa; points are the experimental results, lines are analytical estimations).

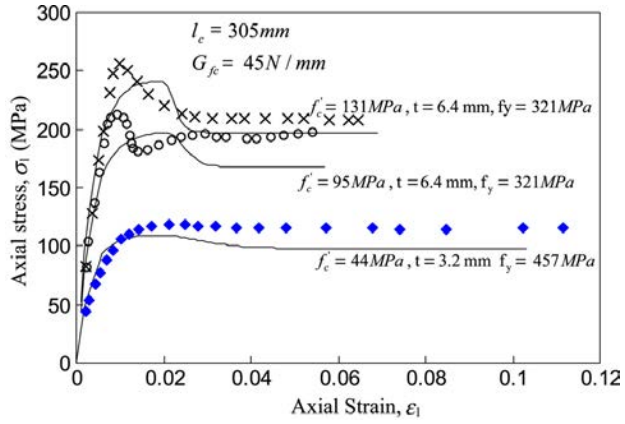

Fig. 10. Comparisons of experimental results of Lahlou et al. [38] with analysis results for concrete confined with steel tubes (points are the experimental results, lines are analytical estimations).

which decreases the yield stress. According to Von Mises plasticity, the modified yield strength of steel loaded in biaxial tension–compression is equal to f_y^* ($f_y^* = f_y/\sqrt{3}$). Using this value for the yield strength of the jacket, analyses were conducted and results compared to the experimental results for three different concrete strengths (Fig. 10). It can be observed that the ultimate and residual strength of the specimens are underestimated by at most about 10%. It should be noted that no contribution of the steel tube in the axial load carrying capacity was considered in the analyses. Therefore, it is possible to say that the model can provide safe and accurate estimations of the capacity for CFSTs where only concrete is loaded in the axial direction.

3.3. FRP confined concrete

Wrapping concrete with fiber reinforced polymers has emerged as one of the most practical ways of increasing the axial load carrying capacity of concrete columns. An extensive database of research exists on FRP wrapped

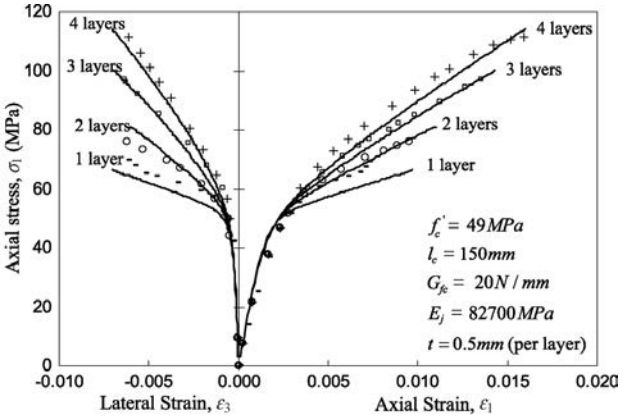

Fig. 11. Comparisons of experimental results of Shahawy et al. [20] with analysis results for concrete confined with FRPs (points are the experimental results, lines are analytical estimations).

cylinders subjected to axial compression. Experiments by Shahawy et al. [20] and Harries and Kharel [39] are selected for comparison against analytical results. The number of unidirectional carbon fiber reinforced polymer layers used to confine the concrete specimens was the test parameter in both studies. Analyses were terminated when the rupture strain of the FRP was reached. Lam and Teng [40] argued that the most suitable test for determining the rupture strain for FRPs was the ring splitting test. In the absence of such tests, on the basis of the statistical analyses of experiments a value equal to about 65% of the rupture strain in direct tension was suggested [40]. Accordingly, the analyses were conducted up to a lateral strain of about 0.007 for the specimens of Shahawy et al. [20] and 0.01 for the specimens of Harries and Kharel [39]. Comparisons of analytical estimations and experimental results are given in Figs. 11 and 12. An excellent agreement can be noted between calculated and observed ultimate capacities. The analytical results closely follow the experimental results reported by Shahawy et al. [20]. The lateral deformations of the specimen with three layers of FRPs [39] were slightly overestimated. Overall, the model can capture the ultimate capacity, lateral deformations, and brittle to ductile failure transition with adequate accuracy.

4. Parametric studies

Parametric studies are conducted in order to investigate the factors that influence the stress–strain behavior of steel and FRP confined concrete. Concrete strength, lateral reinforcement ratio (or the steel tube thickness), and yield strength of steel were the parameters under investigation for steel confined concrete. A concrete cylinder having dimensions of 150 mm × 300 mm was taken as the reference for the parametric studies. Other parameters, the lateral reinforcement ratio, yield strength of the confining reinforcement, and the compressive failure energy, were taken as 0.5%, 414 MPa, and 45 N/mm, respectively.

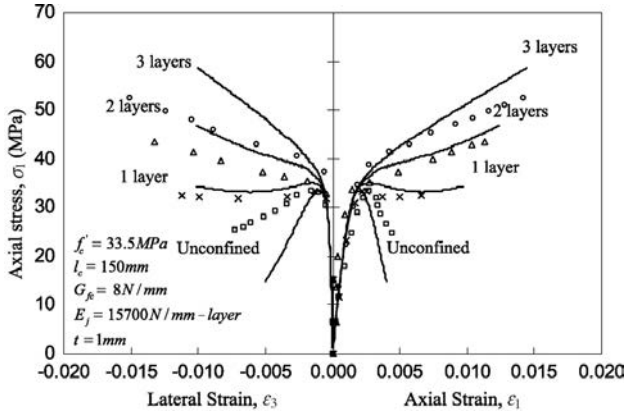

Fig. 12. Comparisons of experimental results of Harries and Kharel [39] with analysis results for concrete confined with FRPs (points are the experimental results, lines are analytical predictions).

First, the effect of uniaxial compressive strength on the stress–strain behavior was investigated. Axial stress–strain curves are presented in Fig. 13(a). It can be observed that peak strength was achieved at similar axial strains when the lateral reinforcement starts yielding. The descending branch of the stress–strain curve showed a steeper descent as the uniaxial compressive strength was increased. Second, the effect of the yield strength of the confining reinforcement is investigated. The yield strength of steel was taken as 414, 828, 1242 MPa. Axial stress–strain results are shown in Fig. 13(b). It can be observed that increase in the yield strength of steel resulted in an increase in ultimate strength and strains at peak strength. However, the slopes of the descending branch of the curves were fairly similar. In all of these analyses, yielding of the reinforcement occurred at peak strength. Finally the effect of the lateral reinforcement ratio on the stress–strain behavior is investigated. Steel tubes made up of high strength steel with a yield strength of 1100 MPa were used in the analyses. The lateral steel ratio was varied from 0.05% to 4% and the rest of the parameters used in the analyses were assumed constant (Fig. 14). It can be observed that for lateral reinforcement ratios smaller than 0.5%, steel yielding occurred after the peak strength was reached. This shows that the assumption of reaching ultimate strength at steel yielding may not always be appropriate, especially for concrete with low confinement provided by high strength steel. The slope of the descending branch was greatly affected by the size of the lateral reinforcement ratio. The stress–strain curves exhibit negligible softening behavior up to very large axial strains when a lateral reinforcement ratio in excess of 4% is provided.

Another set of parametric studies were conducted on FRP confined concrete cylinders. The cylinder dimensions taken were similar to those in the previous study (150 mm × 300 mm). The compressive failure energy was taken as 40 N/mm in the first set of analyses. The FRP jacket was assumed to have a modulus of elasticity of 1.0×10^5 MPa with a varying jacket thickness from 0.02 to

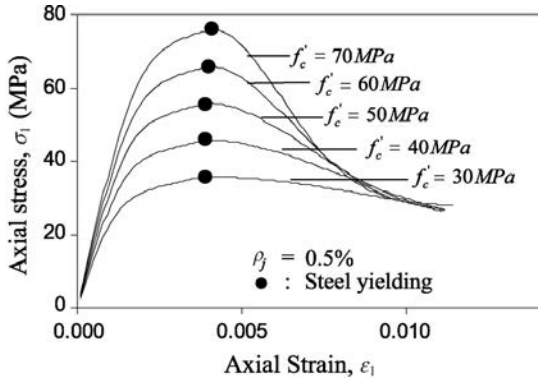

(a) Effect of compressive strength.

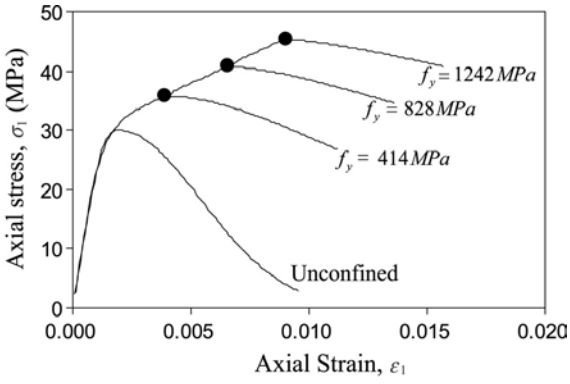

(b) Effect of yield strength.

Fig. 13. Effect of concrete strength and steel yield strength on the behavior of steel confined concrete.

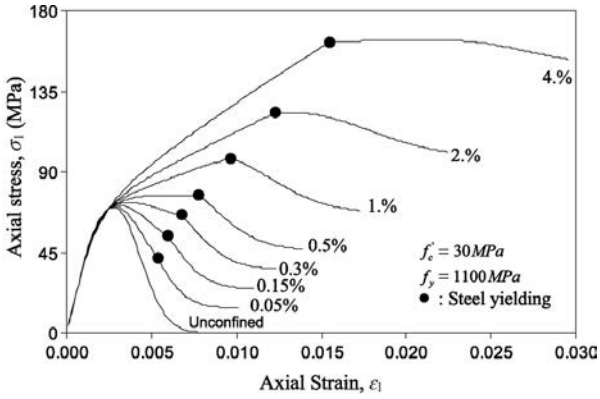

Fig. 14. Effect of lateral reinforcement ratio on the behavior of steel confined concrete (numbers next to curves denote the lateral reinforcement ratio).

0.5 mm. The rupture strain of the jacket is assumed to be 0.01. Analysis results are presented in Fig. 15(a). For FRP thicknesses above 0.05 mm, no softening was observed in the stress–strain response. The strength of FRP wrapped concrete was doubled when a jacket having a thickness of 0.5 mm was used. Another parameter that reveals itself to be important is the compressive failure energy. For the same concrete cylinder having a jacket thickness of 0.05 mm with a modulus of elasticity of 1.0×10^5 MPa, analyses were conducted assuming different compressive failure energies

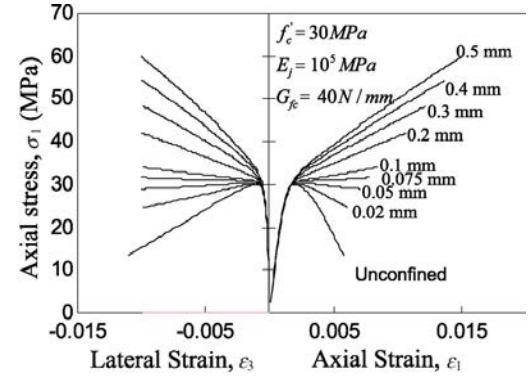

(a) Effect of FRP thickness.

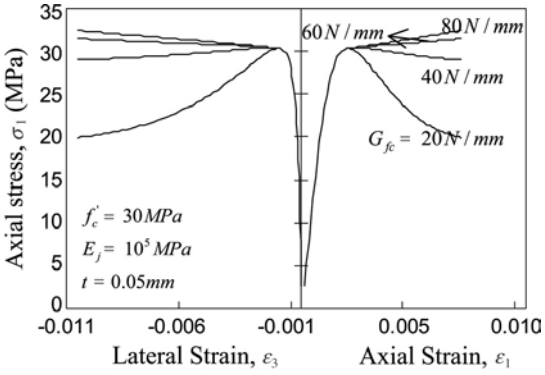

(b) Effect of G_{fc}.

Fig. 15. Effect of FRP thickness and concrete compressive failure energy.

(Fig. 15(b)). It can be seen that the response was quite different for different failure energies. For G_{fc} values greater than 60 N/mm, softening behavior was suppressed with the use of the same jacket thickness. As the slope of the descending region became less steep, the confining stress that would cause a 'no-softening' response could be reached. This, like other factors such as jacket stiffness, lateral reinforcement ratio, and concrete compressive strength, is an important factor influencing the behavior of the jacket for FRP wrapped concrete.

The behaviors of FRP and steel confined concrete having a uniaxial compressive strength of 30 MPa and compressive failure energy of 40 N/mm are compared in Fig. 16 in terms of axial and volumetric behavior. Jacket thicknesses of 1.0 and 0.5 mm were used for steel and FRP confined concrete, respectively. A rupture strain of 0.01 was assumed for the FRP jacket, whereas steel yielding is assumed to occur at 414 MPa. The moduli of elasticity for steel and FRP were taken as 2.0×10^5 and 1.0×10^5 MPa, respectively. It can be observed that the initial stiffnesses and ultimate strengths of steel and FRP confined concrete are similar, but the overall behaviors are significantly different. In the axial direction, the stress–strain response for FRP confined concrete was approximately bilinear, where the degraded stiffness remained constant beyond the uniaxial compressive strength. However, for steel confined concrete, the behavior was nonlinear at first and then an almost perfectly plastic response. Steel confined concrete showed volumetric compaction until

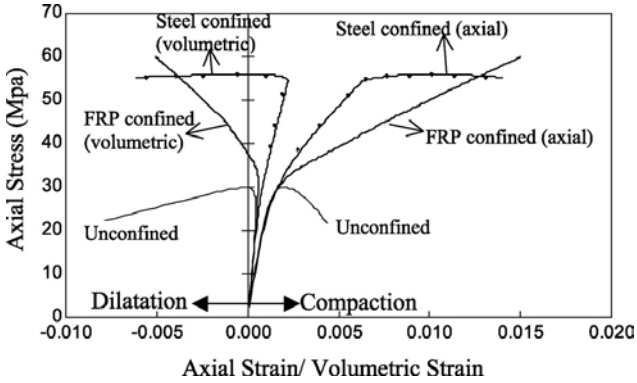

Fig. 16. Comparisons of axial and volumetric behaviors of FRP and steel confined concrete.

ultimate strength was reached, whereas dilatation was observed following that. For FRP confined concrete, the compaction tendency was reversed at about the uniaxial compressive strength. These observations agree well with the experimental comparisons presented by Samaan et al. [41]. The differences in volumetric behavior of the two cases show that application of steel confined concrete models to FRP confined cases requires additional calibration, whereas this need is removed with the proposed model.

5. Summary and conclusions

A new model that is capable of simulating axial and lateral deformations of confined concrete is developed in this study. The model is simple to use as it employs analytical expressions to describe the complete stress–strain curves. The Leon–Pramono criterion [25] is utilized to establish the elastic limit, ultimate strength, and residual capacity of confined concrete. A constant failure energy criterion with an exponential decay function is used to describe the softening behavior. Lateral deformations are explicitly given in terms of axial strains, Poisson's ratio, and secant strain ratios at peak and residual strength. Stress–strain curves for concrete subjected to constant confinement from triaxial compression tests, FRP confined concrete, and concrete confined with spirals and CFSTs where the axial loading is mainly carried by concrete are obtained using the proposed model. Comparisons with the analytical results showed that the model is capable of tracing all essential features of concrete behavior in both directions under compression dominated loadings.

Parametric studies showed that the concrete strength and lateral reinforcement ratio are the two most important factors affecting the descending region of the stress–strain curves for steel confined concrete. The yield strength of steel is found to affect only the ultimate strength. For low levels of confining reinforcement with high strength steel, yielding of steel was observed to occur after the peak strength. For FRP confined concrete it is found that the compressive failure energy can greatly affect whether softening will occur for a small number of FRP layers. It is observed that differences

in volumetric behavior of FRP and steel confined concrete can be captured with the use of the proposed model.

The proposed model offers simplicity in terms of modeling and provides accuracy for a wide range of situations where parametric studies can easily be conducted. The necessity of assuming predetermined stress–strain curves based on assumptions such as yielding of transverse reinforcement or adjusting the softening slope of the stress–strain curves does not arise for the proposed model. Furthermore, the model can provide the equivalent stress–strain response for use in sectional fiber analysis where cage–core interaction can be taken into account. The extension of the model to sections other than circular ones can be performed through the use of confinement effectiveness factors presented in previous studies [14,15]. In its current form, the model is not suitable for cyclic and non-proportional loading cases. However, it can easily be used for capacity and ductility estimations for axially loaded columns and the design of steel or FRPs acting as confining reinforcement.

References

[1] Orito Y, Sato T, Tanaka N, Watanabe Y. Study on the unbonded steel tube composite system. In: Composite construction in steel and concrete proceedings, ASCE engineering foundation. 1987, p. 786–804.

[2] McAteer P, Bonacci JF, Lachemi M. Composite response of high-strength concrete confined by circular steel tube. ACI, Structural Journal 2004;101(4):466–74.

[3] Richart FE, Brandtzaeg A, Brown RL. A study of the failure of concrete under combined compressive stresses. University of Illinois Bulletin 185. 1928, p. 105.

[4] Darwin D, Pecknold DA. Nonlinear biaxial stress–strain law for concrete. Journal of the Engineering Mechanics Division, ASCE 1977;103(2):229–41.

[5] Elwi AA, Murray D. A 3D hypoelastic concrete constitutive relationship. Journal of the Engineering Mechanics Division, ASCE 1979;105(4):623–41.

[6] Ottosen NS. Constitutive model for short-time loading of concrete. Journal of the Engineering Mechanics Division, ASCE 1979;105(2): 127–41.

[7] Madas P, Elnashai S. A new confinement model for the analysis of concrete structures subjected to cyclic and transient dynamic loading. Earthquake Engineering and Structural Dynamics 1992;21:409–31.

[8] Ahmad SH, Shah SP. Stress–strain curves of concrete confined by spiral reinforcement. Journal of the American Concrete Institute 1982; 79(6):484–90.

[9] Smith SS, Willam KJ, Gerstle KH, Sture S. Concrete over the top: Is there life after peak? ACI, Materials Journal 1989;86(5):491–7.

[10] Imran I, Pantazopoulou SJ. Experimental study of plain concrete under triaxial stress. ACI, Materials Journal 1996;93(6):589–601.

[11] Candappa DC, Sanjayan JG, Setunge S. Complete triaxial stress–strain curves of high-strength concrete. Journal of Materials in Civil Engineering, ASCE 2001;13(3):209–15.

[12] Xie J, Elwi AE, MacGregor JG. Mechanical properties of three high strength concretes containing silica fume. ACI Materials Journal 1995;92(2):135–45.

[13] Attard MM, Setunge S. Stress–strain relationship of confined and unconfined concrete. ACI Materials Journal 1996;93(5):432–42.

[14] Sheikh SA, Uzumeri SM. Strength and ductility of tied concrete columns. ASCE, Journal of Structures Division 1980;106(5): 1079–112.

[15] Mander JB, Priestley MJN, Park R. Theoretical stress–strain model for confined concrete. ASCE, Journal of Structural Engineering 1988; 114(8):1804–26.

[16] Scott BD, Park R, Priestley MJN. Stress–strain behavior of concrete confined by overlapping hoops at low and high strain rates. ACI Journal 1982;79(1):13–27.

[17] Razvi S, Saatcioglu M. Confinement model for high strength concrete. ASCE, Journal of Structural Engineering 1999;125(3):281–9.

[18] Assa B, Nishiyama M, Watanabe F. New approach for modeling confined concrete 1: Circular columns. ASCE, Journal of Structural Engineering 2001;127(7):743–50.

[19] Xiao Y, Wu H. Compressive behavior of confined concrete by carbon fiber composite jackets. ASCE, Journal of Materials in Civil Engineering 2000;12(2):139–45.

[20] Shahawy M, Mirmiran A, Beitelman T. Tests and modeling of carbon-wrapped concrete columns. Composites: Part B 2000;31:471–80.

[21] Bazant ZP, Cedolin L. Stability of structures, elastic, inelastic, fracture and damage theories. Mineola (NY): Dover Publications; 2003. p. 1011.

[22] Jansen DC, Shah SP. Effect of length on compressive strain softening of concrete. Journal of Engineering Mechanics 1997;123(1):25–35.

[23] Hatanaka S, Koike S, Mizuno W. Size effects on stress–strain curves of concrete. In: Shing B, Tanabe T, editors. Modeling of inelastic behavior of RC structures under seismic loads. 2001. p. 488–503.

[24] Feenstra PH, De Borst R. A composite plasticity model for concrete. International Journal of Solids and Structures 1996;33(5):707–30.

[25] Pramono E, Willam K. Fracture-energy based plasticity formulation of plain concrete. ASCE, Journal of Engineering Mechanics 1989; 115(8):1183–204.

[26] Etse G, Willam K. Fracture energy formulation for inelastic behavior of plain concrete. ASCE, Journal of Engineering Mechanics 1994; 120:1983–2011.

[27] Pivonka P, Lackner R, Mang HA. Numerical analyses of concrete subjected to triaxial compressive loading. In: European congress on computational methods in applied sciences and engineering. 2000, p. 1–26.

[28] Shah SP, Sankar R. Internal cracking and strain-softening response of concrete under uniaxial compression. ACI Materials Journal 1987; 84(3):200–12.

[29] ACI Committee 318. Building code requirements for structural concrete (ACI 318M-02). Farmington Hills (MI): American Concrete Institute; 2002.

[30] Tasdemir MA, Tasdemir C, Jefferson AD, Lydon FD, Barr BIG. Evaluation of strains at peak stresses in concrete: A three-phase composite model approach. Cement and Concrete Composites 1998; 20:301–18.

[31] Popovics S. A numerical approach to the complete stress–strain curve of concrete. Cement and Concrete Research 1973;3:583–99.

[32] Torrenti JM, Desures J, Benaija EH, Boulay C. Stereophotogrammetry and localization in concrete under compression. ASCE, Journal of Engineering Mechanics 1991;117(7):1455–65.

[33] Cusson D, de Larrard F, Boulay C, Paultre P. Strain localization in confined high-strength concrete columns. ASCE, Journal of Structural Engineering 1996;122(9):1055–61.

[34] Sfer D, Carol I, Gettu R, Etse G. Study of the behavior of concrete under triaxial compression. ASCE, Journal of Engineering Mechanics 2002;128(2):156–63.

[35] Kang HD, Willam KJ. Localization characteristics of triaxial concrete model. ASCE, Journal of Engineering Mechanics 1999;125(8): 941–50.

[36] Yoshikawa H, Yamakawa K. Analysis of inelastic behavior and failure modes of confined concrete by elasto-plastic softening model. In: Shing B, Tanabe T, editors. Modeling of inelastic behavior of RC structures under seismic loads. 2001. p. 79–97.

[37] Borges JUA, Subraminiam KV, Weiss WJ, Shah SP, Bittencourt TN. Length effect on ductility of concrete in uniaxial and flexural compression. ACI Structural Journal 2004;101(6):765–72.

[38] Lahlou K, Lachemi M, Aitcin PC. Behavior of HSC filled tube columns under dynamic compressive loading. ASCE, Journal of Structural Engineering 1999;125(10):1100–8.
[39] Harries KA, Kharel G. Experimental investigation of the behavior of variably confined concrete. Cement and Concrete Research 2003;33: 873–80.
[40] Lam L, Teng JG. Design-oriented stress–strain model for FRP confined concrete. Construction and Building Materials 2003;17: 471–89.
[41] Samaan M, Mirmiran A, Shahawy M. Model of confined concrete by fiber composites. ASCE, Journal of Structural Engineering 1998; 124(9):1025–31.